A Flexible Nanogenerator based on Functionalized Cotton Fibers for Energy Harvesting in Low-Temperature Environment

Si-Zhe Li, Gui-Wen Huang*, Na Li, Yu Liu, Yang Wang, Rui-Xiao Cao, Hong-Mei Xiao**

Video 1: Low-temperature flexibility test process of the flexible conductive fabric.

Video 2: Operation process of the Low-Temperature Triboelectric Performance Tester.

Video 3: Operation of the F-TENG powering the LEDs in low-temperature.

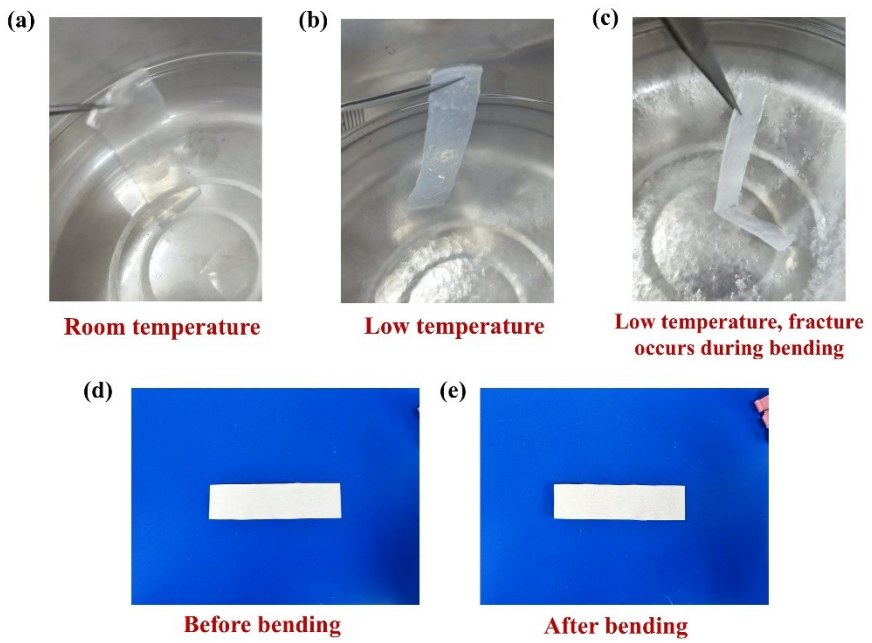

Fig S1 Low-temperature (77K) bending test: (a)(b)(c) Low-temperature bending test of PDMS; (d)(e) Before and after the low-temperature bending test of the cotton fiber film.

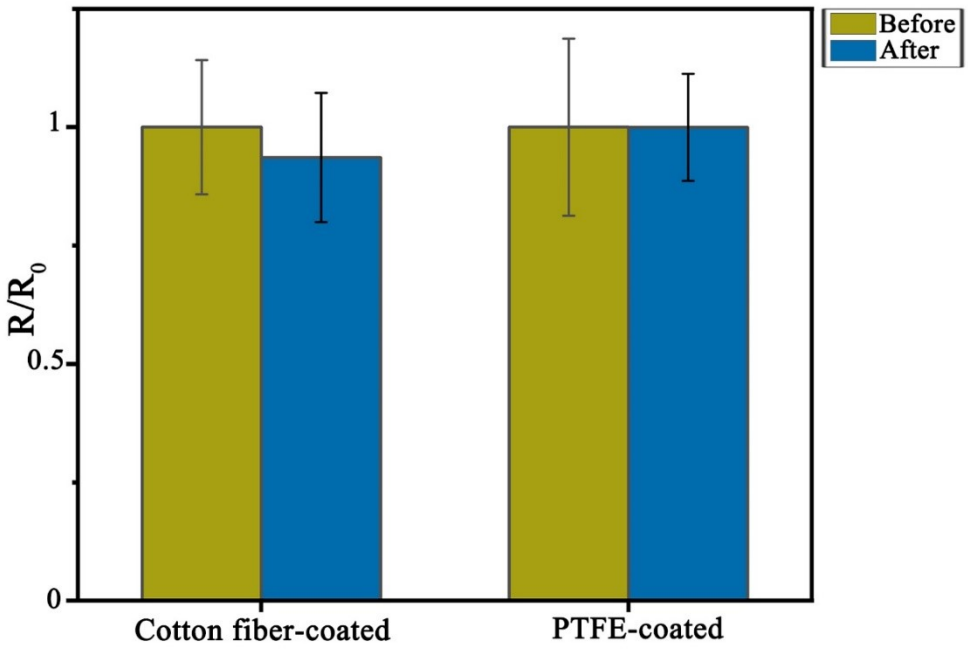

Fig S2 Relative electrical resistance of the FCF, before and after coating with cotton fibers and PTFE.

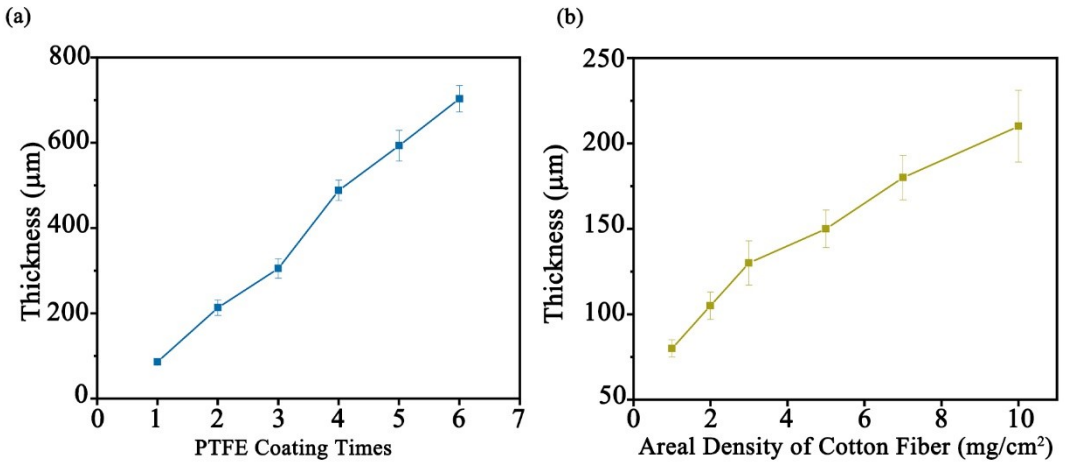

Fig S3 Thickness of friction layer materials in the F-TENG. (a) Variation in thickness of the PTFE-coated friction layer after different dip-and-dried cycles. (b) Variation in thickness of the cotton fiber-coated friction layer at different areal densities.

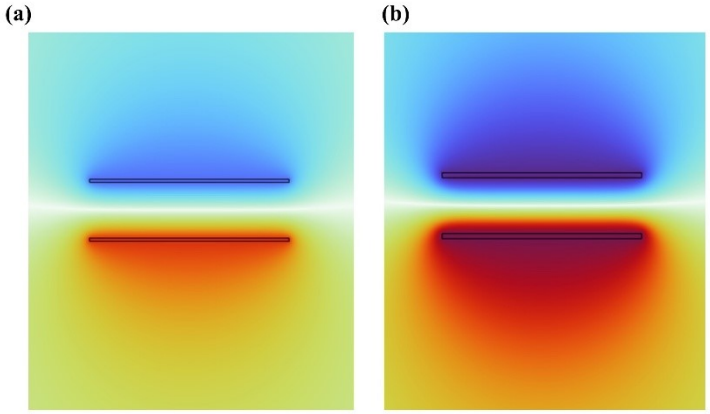

Fig S4 Potential distribution caused by different charge densities.

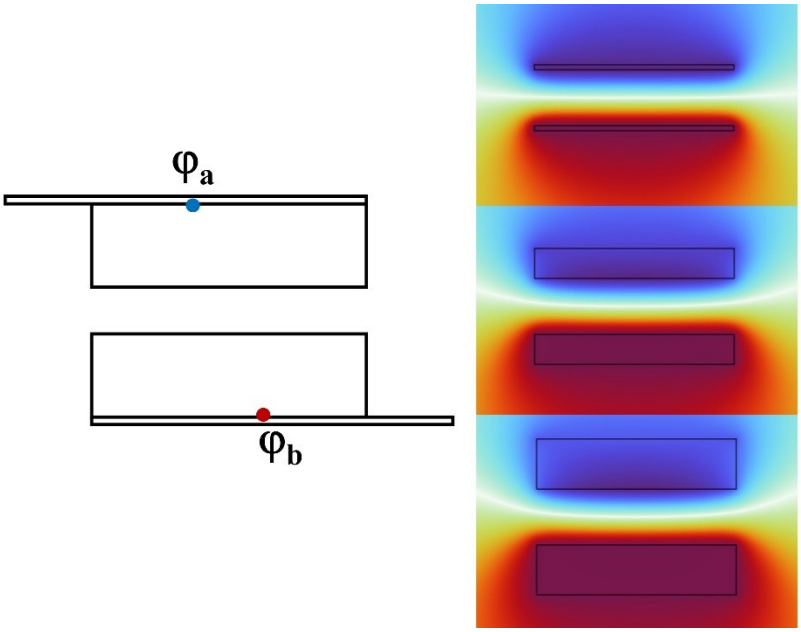

Fig S5 Comparison of the variation in electrostatic induction intensity with increasing thickness of the triboelectric material.

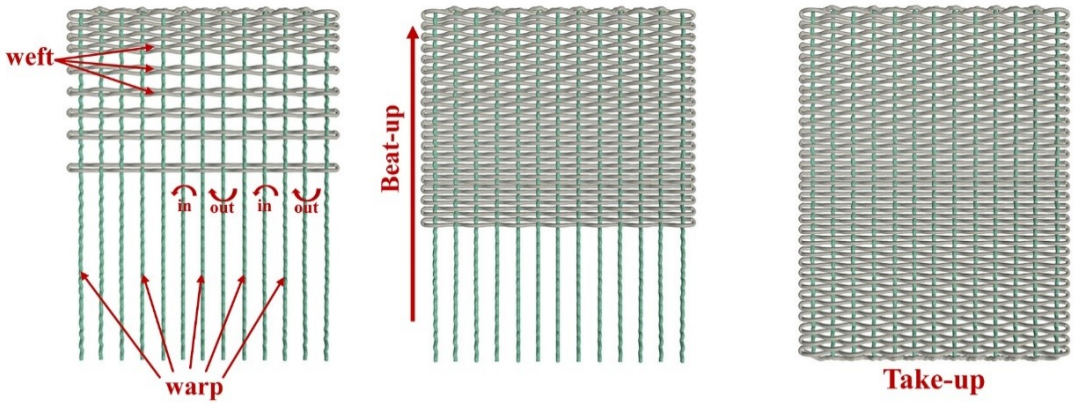

Fig S6 Schematic illustration of the process and operation of the warp and weft weaving method in fabricating of the flexible conductive fabric.

Fig S7 Photograph of the flexible conductive fabric.

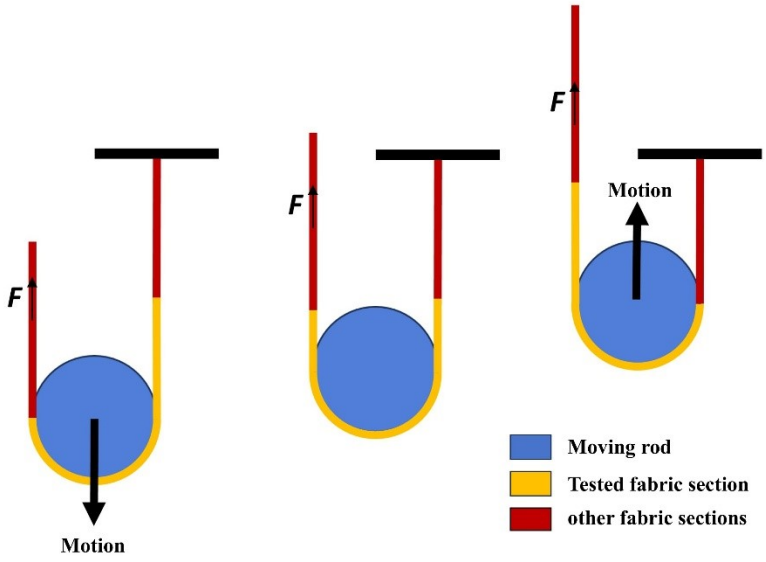

Fig S8 Schematic of the low-temperature flexing test mechanism.

By fixing one end of the tested fabric and applying a constant pulling force to the other end, the moving rod undergoes translational motion, causing different sections of the fabric to wrap around the test rod and undergo bending deformation. This process enables the low-temperature flexibility test.

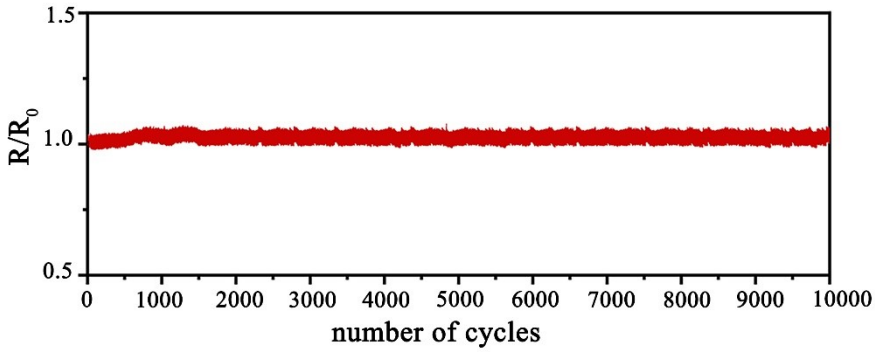

Fig S9 Relative electrical resistance variation of the flexible conductive fabric during 10,000 bending cycles in low-temperature flexibility test.

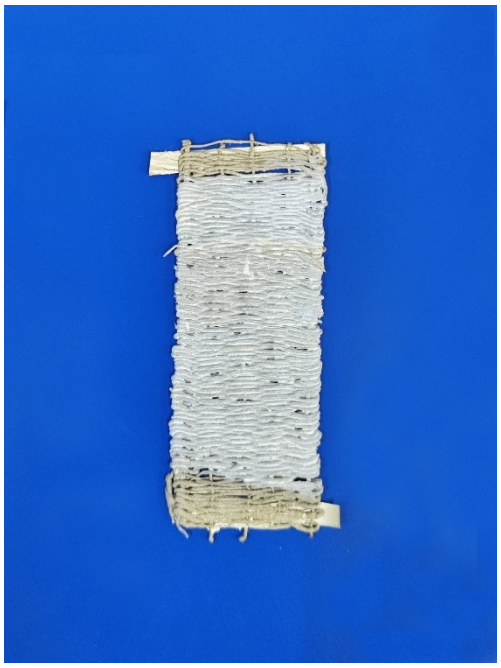

Fig S10 Photograph of the PTFE-coated flexible conductive fabric after 10,000 bending cycles in low-temperature flexibility tests.

Fig S11 Photograph of the cotton fiber-coated flexible conductive fabric after 10,000 bending cycles in low-temperature flexibility tests.

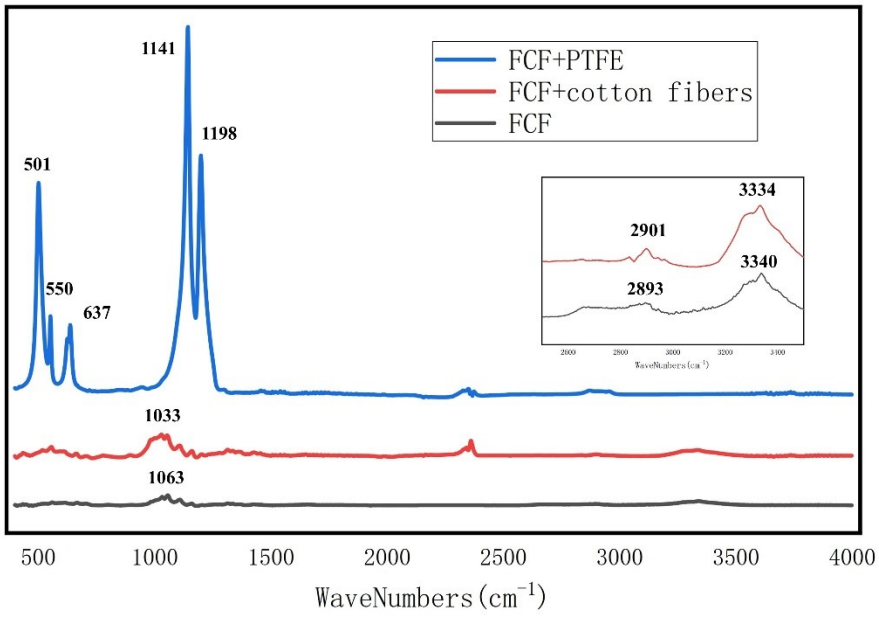

Fig S12 Infrared spectra of flexible conductive fabric, PTFE-coated conductive fabric, and cotton fiber-coated conductive fabric.

Fig. S12 show the infrared spectra of flexible conductive fabric, PTFE-coated conductive fabric, and cotton fiber-coated conductive fabric. FTIR analysis revealed that the main characteristic peaks of cotton fiber and silver nanowire samples include O-H stretching vibration (~3330 cm^{-1}), C-H stretching vibration (~2900 cm^{-1}), C=O stretching vibration (~1730 cm^{-1}), and C-O stretching vibration (~1050 cm^{-1}). However, compared to the coated samples, the IR absorption peaks of cotton fiber and its composite with silver nanowires were relatively weak, making its characteristic absorption peaks less pronounced than those of strongly polar functional groups. After coating with PTFE, the O-H stretching vibration peak slightly shifted, possibly indicating the influence of hydrogen bonding or intermolecular interactions. Additionally, the PTFE-coated sample exhibited a C-F stretching vibration peak at

1200-1100 cm^{-1}, confirming the successful encapsulation of PTFE. The slight shift in the C=O vibration peak may reflect intermolecular interactions, but no significant formation of new chemical bonds was observed. Furthermore, silver nanowires did not exhibit characteristic absorption peaks in the infrared region, suggesting that they primarily exist in a metallic state without significant oxidation or chemical bond changes. Overall, the coating mainly adhered through physical encapsulation and may interact with cotton fibers via hydrogen bonding or van der Waals forces.

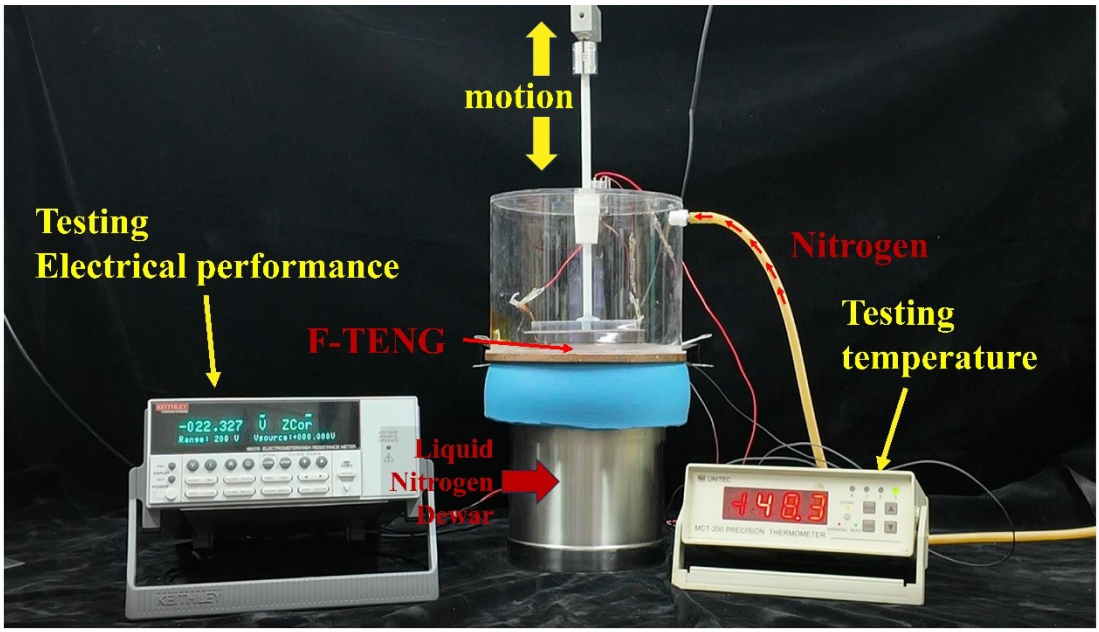

Fig S13 Photo of the Low-Temperature Triboelectric Performance Test system.

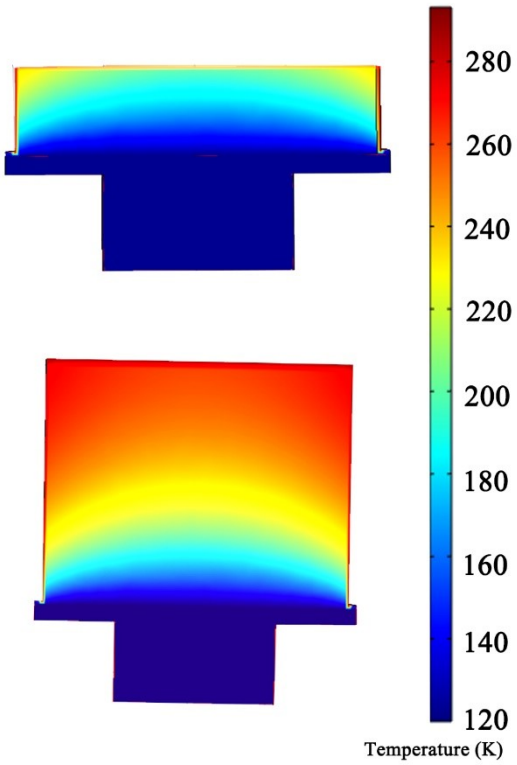

Fig S14 COMSOL-simulated temperature distribution map inside the test sample bin.

In the COMSOL simulation, the enclosure material is set as an acrylic hollow cylinder with outer diameter of 19 cm, inner diameter of 18 cm, wall thickness of 0.5 cm, and height of 18.5 cm. The cooling stage material is set as copper cylinder with upper diameter of 20 cm and height of 1.5 cm, and lower diameter of 10 cm and height of 5 cm. The inner chamber material is set as nitrogen gas with a diameter of 18 cm and a height of 18 cm. For heat transfer settings: the enclosure and cooling stage are defined as solids, while the inner chamber is defined as a fluid. The temperature settings are as follows: the bottom surface of the cooling stage is set to 77 K, and the outer wall of the enclosure is set to 293.15 K.

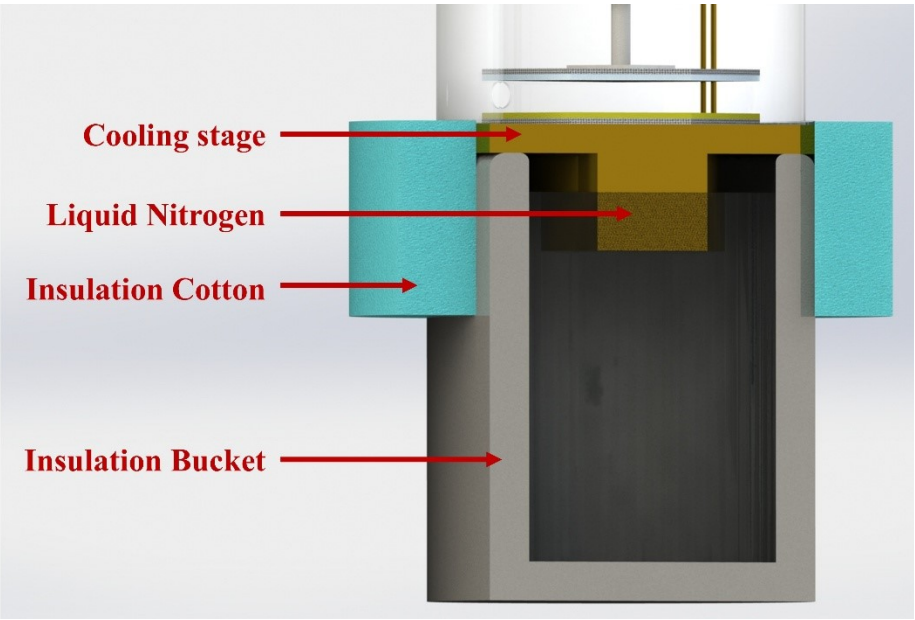

Fig S15 Model of the cooling device in the test setup.

Liquid nitrogen is stored in an insulated bucket with inner diameter of 16 cm, outer diameter of 20 cm, and depth of 21 cm. The cooling stage is a convex cylinder made of copper, with upper diameter of 20 cm and height of 1.5 cm, and lower diameter of 10 cm and height of 5 cm.

During the cooling process, liquid nitrogen is added to the insulated bucket, submerging the lower part of the cooling stage. This allows the device to cool rapidly, and the temperature of the cooling stage is adjusted by controlling the amount of liquid nitrogen added, and the temperature of the upper stage of the copper is monitored in real time. Due to the high thermal capacity of copper, the test temperature can remain stable for an extended period.

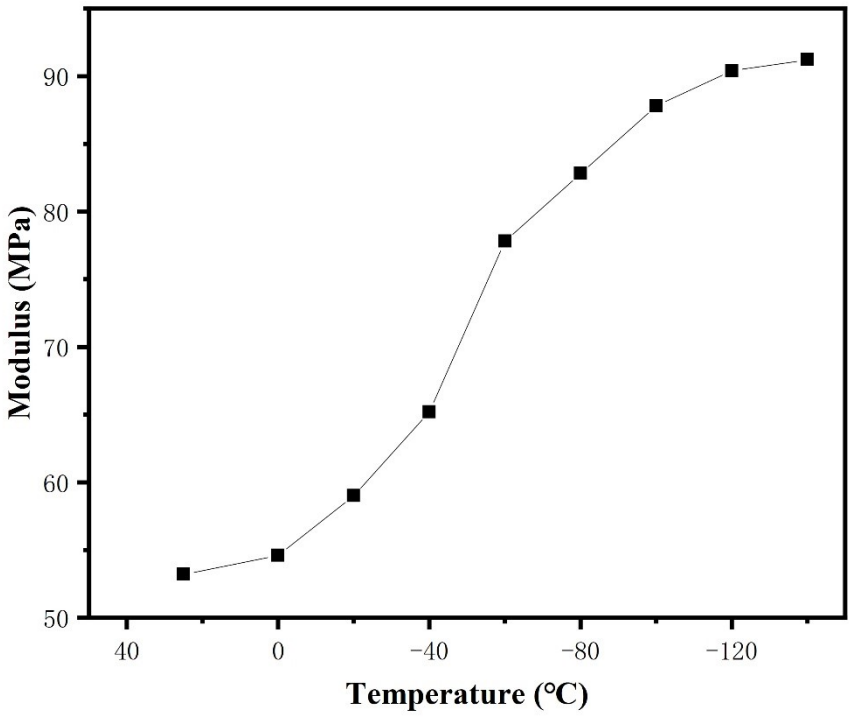

Fig S16 Variation of cotton fiber flexural modulus with decreasing temperature.

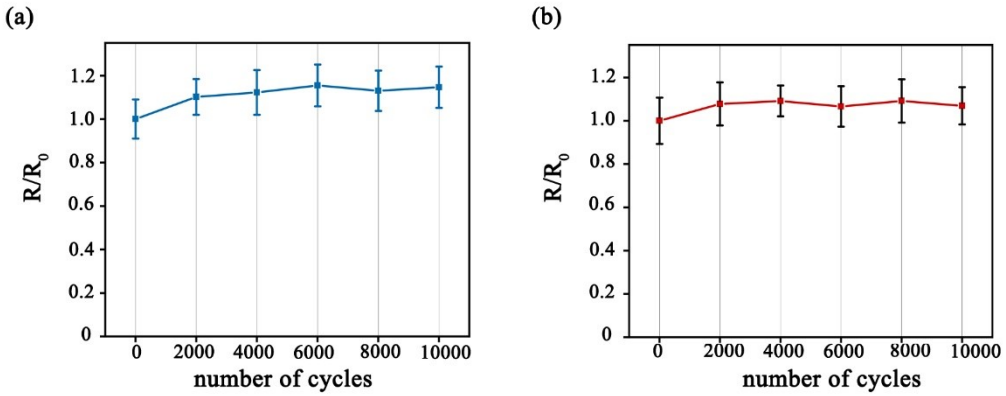

Fig S17 Resistance of (a)PTFE (b)cotton fibers variation at intervals of 2000 low-temperature flexibility testing cycles.

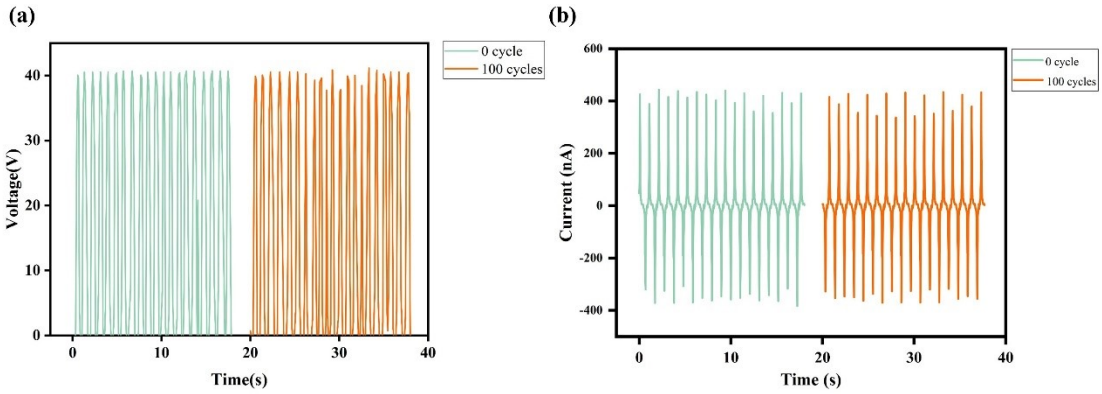

Fig S18 Performance comparison before and after 100 times of thermal shock（25℃ to -196℃）: (a) Voltage, (b) Current.

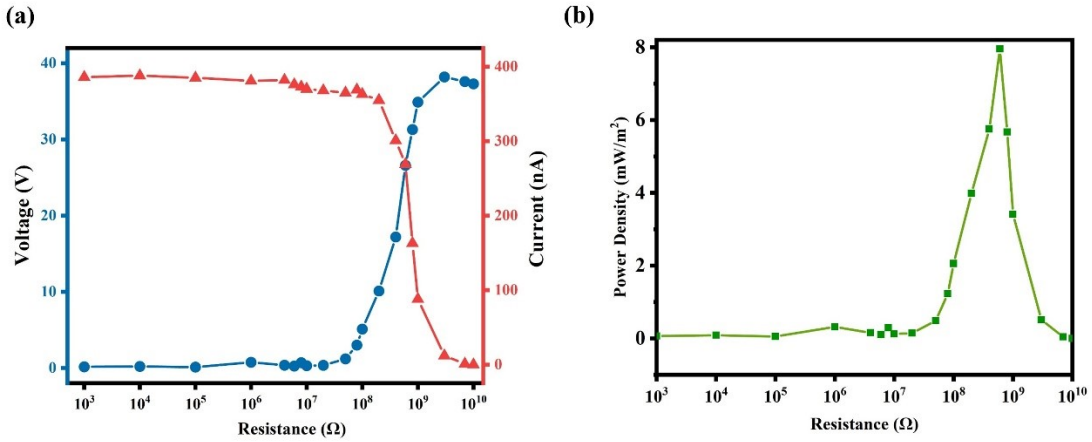

Fig S19 Variation of the output performance with different external resistances. (a) voltage, current (b) power density.

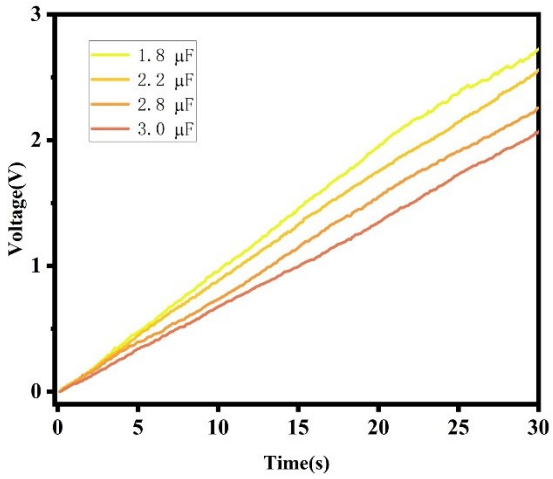

Fig S20 Charging voltage curves of the FT-TENG for different capacitors.

Table S1 Comparison of output performance and minimum operating temperature of this work and techniques in literatures.

Material Composition	**minimum operating temperature (℃)**	**Power Density (μW/cm²)**	**Ref.**
polyurethane/cellulose nanofiber supramolecular elastomer	-10	0.7	[1]
polyurethane elastomers/glycerol/polycaprolactone	-30	1.4	[2]
cellulose organohydrogels	-24	334.8	[3]
PAzo-co-polystyrene/ nylon fabrics	-20	250	[4]
PPAVC-BA ionic hydrogel/CNF	-50	200	[5]
PBES-U (prepared from biobased monomers such as itaconic acid, sebacic acid, etc.)	-40	1.2	[6]
Poly (Low Molecular weight Biobased Elastomer)	-10	0.225	[7]
Cotton Fiber + Silver Nanowires/PTFE/Cotton Fiber Composite	-130	0.79	This work

Reference

[1] Wang H, Zhao Z, Zhang L, et al. High-performance low-temperature self-healing bio-based polyurethane triboelectric nanogenerator for wireless intelligent target systems [J]. Nano Energy, 2025, 133.

[2] Wang H, Gao M, Zhang L, et al. Advanced low-temperature self-healable bio-polyurethanes with double-alkane-tailed ringing units for applications in self-powered flexible control panels [J]. Chem Eng J, 2025, 506.

[3] Qin C, Lu A. Flexible, anti-freezing self-charging power system composed of cellulose based supercapacitor and triboelectric nanogenerator [J]. Carbohydr Polym, 2021, 274: 118667.

[4] Zheng X, Dai X, Ge J, et al. Self-regulating heating and self-powered flexible fiber fabrics at low temperature [J]. J Mater Sci Technol, 2025, 220: 104-14.

[5] Lei T, Wang Y, Zhang Q, et al. Ultra-stretchable and anti-freezing ionic conductive hydrogels as high performance strain sensors and flexible triboelectric nanogenerator in extreme environments [J]. Nano Energy, 2024, 126.

[6] Wang H, Zhang L, Su Z, et al. Bio-based polyurethane triboelectric nanogenerator with superior low-temperature self-healing performance for unmanned surveillance [J]. Nano Energy, 2024, 130.

[7] Wang H, Yin Y, Su Z, et al. Bio-Based and Recyclable Self-Healing Elastomer for the Application of Self-Powered Triboelectric Nanogenerator in Low-Temperature [J]. Adv Funct Mater, 2024, 34(11): 2311649.